Accuracy of Angle Estimation in eCompass and 3-D Pointer Applications

by: Talat Ozyagcilar
Applications Engineer

1 Introduction

This application note addresses the relationship between errors in the outputs from accelerometer and magnetometer sensors and the resulting errors in the roll, pitch and yaw angles computed by a tilt-compensated eCompass or 3-D Pointer application.

The mathematical approach continues that developed in Freescale Application Notes AN4248 "Implementing a Tilt-Compensated eCompass using Accelerometer and Magnetometer Sensors", AN4246 "Calibrating an eCompass in the Presence of Hard and Soft Iron Interference" and AN4247 "Layout Recommendations for PCBs Using a Magnetometer Sensor". It is recommended that these are read first to provide the mathematical foundation for this document.

The error analysis starts by determining the relationship between accelerometer errors and errors in the estimated roll and pitch angles. The consequent error in compass angle is then derived from the roll and pitch angle errors. Expressions are then derived for the errors in the compass heading angle resulting from errors in the

Contents

freescale
Xtrinsic

magnetometer sensor and the hard and soft iron calibration. The final section extends the discussion to the statistics of time varying sensor outputs.

To avoid unnecessarily complex phrasing, the term "compass heading" is used throughout to refer to the yaw angle. Where small angle approximations are used, it should be assumed that the angle is measured in radians.

1.1   Key Words

Accelerometer, Magnetometer, eCompass, 3-D Pointer, Angle Error, Hard Iron, Soft Iron.

1.2   Summary

- The accelerometer sensor output is used by the tilt-compensated eCompass algorithms to compute the roll and pitch angles. Errors in the accelerometer output therefore create errors in the computed roll and pitch angles. With a small angle approximation, the roll and pitch angle errors are roughly equal to the ratio of the accelerometer errors to the gravitational acceleration g.

- Errors in the estimated roll and pitch angles lead to an error in the estimated compass angle. With a small angle approximation, the compass angle error is approximately equal to the square root of the sum of the squares of the roll and pitch angle errors.

- An instability in the roll angle calculation exists when the PCB is held at a pitch angle closer to vertical than the ratio of the z-channel accelerometer error to g. This leads directly to an instability in the compass angle if workarounds are not deployed.

- The sum of the magnetometer zero field offset and the hard and soft iron magnetic interference created by ferromagnetic components on the PCB will typically dominate the geomagnetic field and completely jam an eCompass if software calibration algorithms are not deployed.

- Any inaccuracy in the estimated magnetometer zero field offset and hard iron calibration will leave a residual fixed magnetic offset which manifests as a compass heading error varying sinusoidally with one error cycle per 360° rotation in compass heading. The amplitude of this compass heading error is equal to the ratio of the square root of the sum of the squares of the residual hard iron error to the horizontal geomagnetic field component.

- Any inaccuracy in the soft iron calibration will leave a residual directional distortion of the geomagnetic field which manifests as a compass heading error also varying sinusoidally with compass heading but with two error cycles per 360° rotation in compass heading.

2   Angle Estimation in the eCompass and 3-D Pointer

The tilt-compensated eCompass uses the combination of a three axis accelerometer and a three axis magnetometer in a six degree of freedom system. Calibration algorithms correct the magnetometer readings for hard and soft iron interference generated by ferromagnetic components on the PCB. The accelerometer output is used to correct the magnetometer output in roll and pitch angles after which the final compass heading is computed.

Since the tilt-compensated eCompass algorithms compute all three roll, pitch and compass angles, the eCompass can also be used to implement a 3-D remote control pointer. Typically the compass heading and

pitch angles are used to define the pointing direction in the horizontal and vertical axes respectively. Full details are provided in application note AN4248.

3 Accelerometer Induced Errors in Roll and Pitch Angles

This section calculates the errors in the computed roll ϕ and pitch θ angles as a function of errors in the three accelerometer components.

Equation 3 in application note AN4248 gives the accelerometer output G_p at true orientation angles ϕ_0 and θ_0 as a function of the rotation matrices $R_x(\phi_0)$ and $R_y(\theta_0)$ defined in AN4248 equations 5 and 6. Adding an accelerometer error vector $\{\Delta G_{px}, \Delta G_{py}, \Delta G_{pz}\}$ extends AN4248 equation 3 to:

$$G_p = \begin{pmatrix} G_{px} \\ G_{py} \\ G_{pz} \end{pmatrix} = R_x(\phi_0)R_y(\theta_0)\begin{pmatrix} 0 \\ 0 \\ g \end{pmatrix} + \begin{pmatrix} \Delta G_{px} \\ \Delta G_{py} \\ \Delta G_{pz} \end{pmatrix} = \begin{pmatrix} -g\sin\theta_0 + \Delta G_{px} \\ g\cos\theta_0\sin\phi_0 + \Delta G_{py} \\ g\cos\theta_0\cos\phi_0 + \Delta G_{pz} \end{pmatrix} \qquad \textbf{\textit{Eqn. 1}}$$

In application note AN4248, equation 13 defines the estimated roll angle ϕ in terms of the two accelerometer components G_{py} and G_{pz}.

$$\tan\phi = \left(\frac{G_{py}}{G_{pz}}\right) \qquad \textbf{\textit{Eqn. 2}}$$

Combining Equations 1 and 2 gives an explicit expression for the error $\Delta\phi$ in the estimated roll angle in terms of four variables: the true pitch and roll orientation angles θ_0, ϕ_0 and the y- and z-channel accelerometer errors ΔG_{py}, ΔG_{pz}:

$$\Delta\phi = \phi - \phi_0 = \tan^{-1}\left(\frac{G_{py}}{G_{pz}}\right) - \phi_0 = \tan^{-1}\left(\frac{g\cos\theta_0\sin\phi_0 + \Delta G_{py}}{g\cos\theta_0\cos\phi_0 + \Delta G_{pz}}\right) - \phi_0 \qquad \textbf{\textit{Eqn. 3}}$$

For the special case where $\Delta G_{pz} = 0$ (no z-channel accelerometer noise) and $\theta_0 = 0$ (no pitch rotation), Equation 3 simplifies to:

$$\Delta\phi = \phi - \phi_0 = \tan^{-1}\left(\frac{g\sin\phi_0 + \Delta G_{py}}{g\cos\phi_0}\right) - \phi_0 \qquad \textbf{\textit{Eqn. 4}}$$

Application Note AN4248, equation 15 defines the estimated pitch angle θ in terms of the three accelerometer components G_{px}, G_{py} and G_{pz} and the estimated roll angle ϕ:

$$\tan\theta = \left(\frac{-G_{px}}{G_{py}\sin\phi + G_{pz}\cos\phi}\right) \qquad \textbf{\textit{Eqn. 5}}$$

Combining equations 1 and 5 gives the expression for the error $\Delta\theta$ in the estimated pitch angle:

$$\Delta\theta = \theta - \theta_0 = tan^{-1}\left(\frac{g\sin\theta_0 - \Delta G_{px}}{(g\cos\theta_0\sin\phi_0 + \Delta G_{py})\sin\phi + (g\cos\theta_0\cos\phi_0 + \Delta G_{pz})\cos\phi}\right) - \theta_0 \qquad \textbf{\textit{Eqn. 6}}$$

For the special case where $\Delta G_{py} = \Delta G_{pz} = 0$ (no y- or z-channel accelerometer noise present) and $\phi = \phi_0 = 0$ (no roll rotation), Equation 6 simplifies to:

$$\Delta\theta = \theta - \theta_0 = tan^{-1}\left(\frac{g\sin\theta_0 - \Delta G_{px}}{g\cos\theta_0}\right) - \theta_0 \qquad \textbf{\textit{Eqn. 7}}$$

Equations 4 and 7 are identical in form, apart from a sign difference in the terms ΔG_{px} and ΔG_{py}. Figure 1 shows the form of both equations as a function of accelerometer error ΔG_{px} and ΔG_{py}, varying from 0 mg to 100 mg. The peak error occurs near zero roll or pitch angle with value (in radians) equal to the ratio of the accelerometer noise component to g.
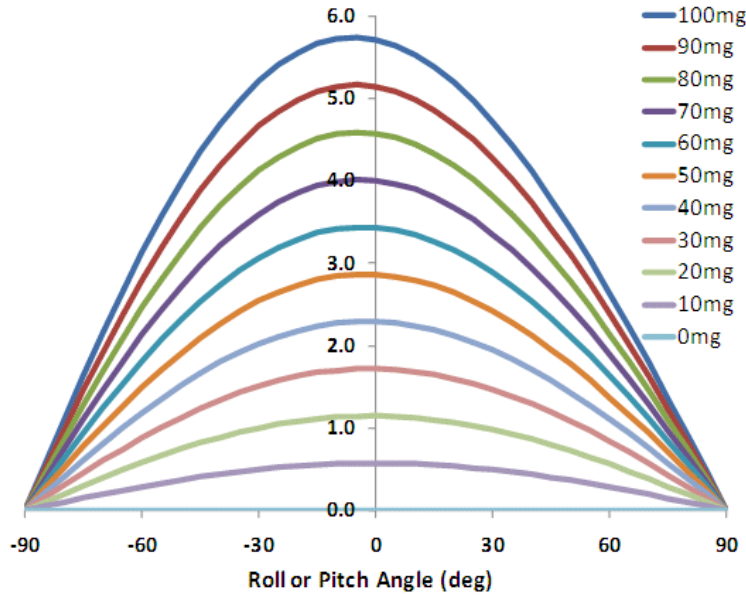
Figure 1. Angle Error (degrees) for G_{py} (Roll) and G_{px} (Pitch) Errors

Equation 3 can be similarly simplified for the special cases of zero pitch angle $\theta_0 = 0$ and Equation 6 for zero roll angle $\phi_0 = 0$ with accelerometer error in the z-axis only to give:

$$\Delta\phi = \phi - \phi_0 = tan^{-1}\left(\frac{g\sin\phi_0}{g\cos\phi_0 + \Delta G_{pz}}\right) - \phi_0 \qquad \textbf{\textit{Eqn. 8}}$$

$$\Delta\theta = \theta - \theta_0 = tan^{-1}\left(\frac{g\sin\theta_0}{g\cos\theta_0 + \Delta G_{pz}}\right) - \theta_0 \qquad \textbf{\textit{Eqn. 9}}$$

Equations 8 and 9 have a similar form and are plotted together in Figure 2 for the z-axis accelerometer error ΔG_{pz} varying between 0 and 100 mg. In this case, the z-axis accelerometer error has least impact at

flat orientation and has most impact at pitch and roll angles near 90° where the z-axis accelerometer reading approaches zero and is dominated by the error ΔG_{pz}. Using the relation $tan^{-1}(x) = \pi/2 - tan^{-1}(1/x)$, the error at $90°$ equals the ratio of the z-channel noise ΔG_{pz} to g.
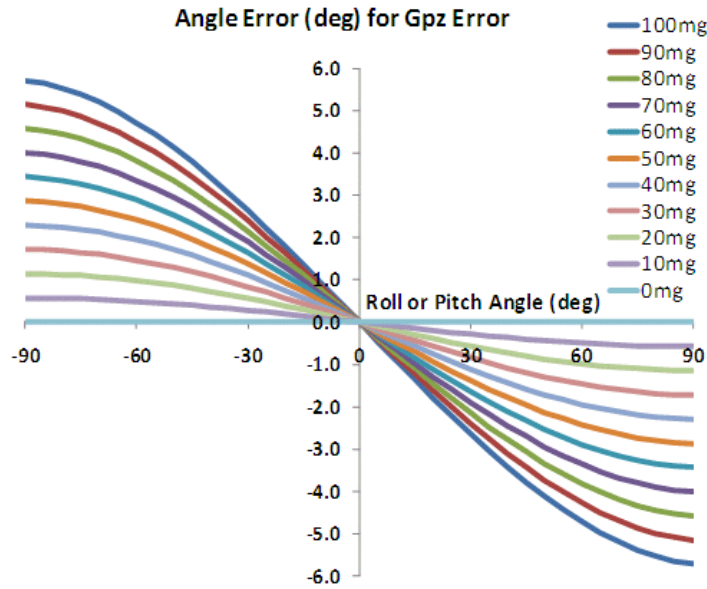

Figure 2. Error in Roll and Pitch Angle as a Function of G_{pz} Errors

4   Instabilities in Roll and Pitch Angle Estimation

The previous section determined the errors in the roll and pitch angle as a function of accelerometer errors when the other angle (pitch or roll respectively) was zero. Figures 1 and 2 show that the errors in the estimated angles are numerically well behaved in these special cases. This section investigates whether there are orientations where the roll and pitch angles become unstable and infinitely sensitive to accelerometer errors.

The estimated roll angle ϕ is defined by Equation 2 in terms of the measured y and z-accelerometer outputs. Simple inspection of Equation 2 indicates that:

i) The estimated roll angle is well behaved for all G_{py}, when G_{pz} is not near zero. Zero G_{py} gives an estimated roll angle of zero.

ii) The estimated roll angle is also well behaved for all G_{pz}, when G_{py} is not near zero. Zero G_{pz} gives an estimated roll angle of -90° or 90°.

iii)The estimated roll angle is, however, unstable when both G_{py} and G_{pz} are near zero. The estimated roll angle is essentially random in the range -180° to 180°.

The third case corresponds to the eCompass pointed vertically upwards at 90° pitch angle or vertically downwards at -90° pitch angle. The accelerometer is then insensitive to any rotation in roll since the roll axis is aligned with the gravitation vector and both G_{py} and G_{pz} are zero irrespective of roll angle.

Since the roll angle is used to de-rotate the magnetometer reading, the instability in the estimated roll angle also leads directly to an instability in the compass angle.

This can be understood in the mathematics of the rotation matrix sequence defined in AN4248. Expanding the product of the three rotation matrix sequence when the compass is vertical at $\theta_0 = 90^o$ gives:

$$\boldsymbol{R}_x(\phi_0)\boldsymbol{R}_y\left(\theta_0 = \frac{\pi}{2}\right)\boldsymbol{R}_z(\psi_0) = \begin{pmatrix} 1 & 0 & 0 \\ 0 & \cos\phi_0 & \sin\phi_0 \\ 0 & -\sin\phi_0 & \cos\phi_0 \end{pmatrix} \begin{pmatrix} 0 & 0 & -1 \\ 0 & 1 & 0 \\ 1 & 0 & 0 \end{pmatrix} \begin{pmatrix} \cos\psi_0 & \sin\psi_0 & 0 \\ -\sin\psi_0 & \cos\psi_0 & 0 \\ 0 & 0 & 1 \end{pmatrix} \qquad \textbf{\textit{Eqn. 10}}$$

$$= \begin{pmatrix} 0 & 0 & -1 \\ -\sin(\psi_0-\phi_0) & \cos(\psi_0-\phi_0) & 0 \\ \cos(\psi_0-\phi_0) & \sin(\psi_0-\phi_0) & 0 \end{pmatrix} = \boldsymbol{R}_y\left(\theta_0 = \frac{\pi}{2}\right)\boldsymbol{R}_z(\psi_0-\phi_0) \qquad \textbf{\textit{Eqn. 11}}$$

Equation 11 states that when the compass is vertical, any rotation in roll adds to compass angle. Any error in the estimated roll angle therefore leads to an identical error in the estimated compass heading. The same mathematics applies when the eCompass is pointing downwards at $\theta_0 = -90^o$.

In practice this roll instability is more of a theoretical problem than a practical problem. A simple workaround is to mix approximately 5% of G_{px} into the denominator of Equation 2 in order to smoothly drive the roll angle to zero at near vertical operation. This stabilizes the eCompass and has the additional benefit of changing the compass pointing direction to align with the *z*-axis, exactly as would be expected by a user holding up an eCompass vertically. Equation 2 with this workaround then becomes:

$$\tan\phi = \left(\frac{G_{py}}{G_{pz} + \alpha G_{px}}\right) \text{ with } \alpha \approx 5\% \qquad \textbf{\textit{Eqn. 12}}$$

The pitch angle θ_0 at which the calculation of the roll angle ϕ becomes unstable, assuming that the workaround in Equation 12 is not used, is given by the *z* component of Equation 1 as:

$$\theta_0 = \cos^{-1}\left|\frac{\Delta G_{pz}}{g}\right| \Rightarrow \left(\frac{\pi}{2}\right) - \theta_0 \approx \sin^{-1}\left|\frac{\Delta G_{pz}}{g}\right| = \left|\frac{\Delta G_{pz}}{g}\right| \text{for small } \theta_0 \qquad \textbf{\textit{Eqn. 13}}$$

Equation 13 is plotted for θ_0 in Figure 3. The behavior is physically realistic decreasing from 90° for no accelerometer error to 0° as the *z*-channel error approaches 1g.
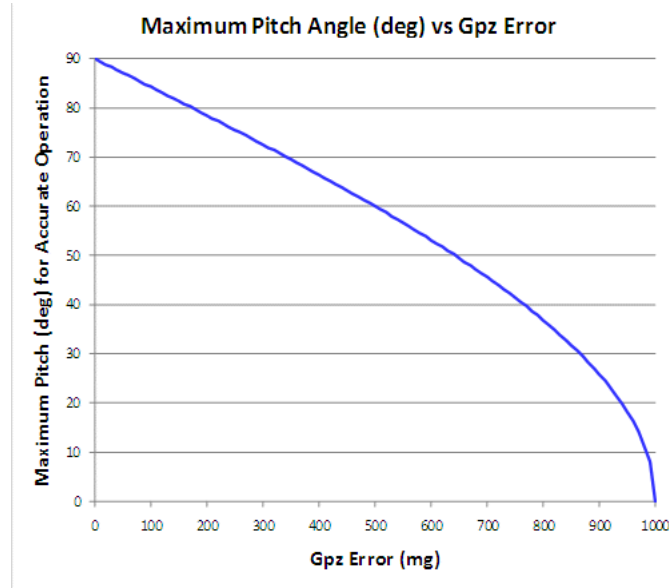
Figure 3. Maximum eCompass Pitch Angle versus G$_{pz}$ Error

No such instabilities occur in the calculation of the pitch angle using Equation 5. This can be proved by substituting the two trigonometric identities with Equations 2 and 5:

$$sin\,\phi = \left(\frac{\pm tan\,\phi}{\sqrt{1 + tan^2\phi}} \right) \qquad\qquad \textbf{Eqn. 14}$$

$$cos\,\phi = \left(\frac{\pm 1}{\sqrt{1 + tan^2\phi}} \right) \qquad\qquad \textbf{Eqn. 15}$$

$$tan\,\theta = \left(\frac{-G_{px}}{G_{py}\left(\frac{tan\,\phi}{\sqrt{1 + tan^2\phi}}\right) + G_{pz}\left(\frac{1}{\sqrt{1 + tan^2\phi}}\right)} \right) = \left(\frac{-G_{px}}{\sqrt{G_{py}^{\;2} + G_{pz}^{\;2}}} \right) \qquad\qquad \textbf{Eqn. 16}$$

Applying the additional constraint that the modulus of the accelerometer output equals the gravitational acceleration *g*:

$$G_{px}^{\;2} + G_{py}^{\;2} + G_{pz}^{\;2} = g^2 \qquad\qquad \textbf{Eqn. 17}$$

gives:

$$tan\,\theta = \left(\frac{-G_{px}}{\sqrt{g^2 - G_{px}^{\;2}}} \right) \qquad\qquad \textbf{Eqn. 18}$$

It is impossible for both numerator and denominator in Equation 18 to be simultaneously zero. The pitch angle θ_0 calculation is therefore stable under all circumstances.

5　Accelerometer Induced Errors in the Compass Angle

The previous sections have derived expressions for the errors in roll and pitch angles as a function of accelerometer errors. These pitch and roll angle errors lead to an error in the compass angle even before the magnetometer data is used.

AN4248 equation 4 gives the magnetometer output $\boldsymbol{B}_p$ (ignoring any magnetometer error and any hard or soft iron interference for now) in terms of the true orientation angles and the magnetic inclination angle δ as:

$$\boldsymbol{B}_p = \begin{pmatrix} B_{px} \\ B_{py} \\ B_{pz} \end{pmatrix} = \boldsymbol{R}_x(\phi_0)\boldsymbol{R}_y(\theta_0)\boldsymbol{R}_z(\psi_0)B\begin{pmatrix} cos\,\delta \\ 0 \\ sin\,\delta \end{pmatrix} \qquad \textit{\textbf{Eqn. 19}}$$

After correction for the estimated roll and pitch angles, the de-rotated magnetometer output is:

$$\boldsymbol{R}_y(-\theta)\boldsymbol{R}_x(-\phi)\boldsymbol{B}_p = \boldsymbol{R}_y(\theta_0-\theta)\boldsymbol{R}_x(\phi_0-\phi)\boldsymbol{R}_z(\psi_0)B\begin{pmatrix} cos\,\delta \\ 0 \\ sin\,\delta \end{pmatrix} \qquad \textit{\textbf{Eqn. 20}}$$

$$= \boldsymbol{R}_y(-\Delta\theta)\boldsymbol{R}_x(-\Delta\phi)B\begin{pmatrix} cos\,\psi_0 cos\,\delta \\ -sin\,\psi_0 cos\,\delta \\ sin\,\delta \end{pmatrix} \approx B\begin{pmatrix} cos\,\psi_0 cos\,\delta + \Delta\theta sin\,\delta \\ -sin\,\psi_0 cos\,\delta - \Delta\phi sin\,\delta \\ -\Delta\theta cos\,\psi_0 cos\,\delta - \Delta\phi sin\,\psi_0 cos\,\delta + sin\,\delta \end{pmatrix} \qquad \textit{\textbf{Eqn. 21}}$$

AN4248 equations 20 to 22 give an expression for the estimated compass angle ψ as the negative ratio of the y and x tilt-compensated magnetometer readings. Substituting the components of Equation 21 gives:

$$tan\,\psi = tan(\psi_0 + \Delta\psi) = \left(\frac{sin\,\psi_0 + \Delta\phi tan\,\delta}{cos\,\psi_0 + \Delta\theta tan\,\delta}\right) \Rightarrow \Delta\psi = tan^{-1}\left(\frac{sin\,\psi_0 + \Delta\phi tan\,\delta}{cos\,\psi_0 + \Delta\theta tan\,\delta}\right) - \psi_0 \qquad \textit{\textbf{Eqn. 22}}$$

Figure 4 shows the Equation 22 geometrically. Simple inspection shows that the error $\Delta\psi$ will vary sinusoidally with true compass angle ψ_0 and that (assuming $\Delta\phi tan\,\delta$ and $\Delta\theta tan\,\delta$ are much less than unity) the maximum value of $\Delta\psi$ will have value in radians given by:

$$\Delta\psi_{max} = \sqrt{(\Delta\phi tan\,\delta)^2 + (\Delta\theta tan\,\delta)^2} \qquad \textit{\textbf{Eqn. 23}}$$

It should be noted that the small angle approximation used in Equation 23 breaks down near the geomagnetic poles where $tan\,\delta$ is unbounded.

The compass error angle $\Delta\psi$ will equal zero at true angles ψ_0 where:

$$tan(\psi_0) = \frac{\Delta\phi\, tan\,\delta}{\Delta\theta\, tan\,\delta} = \frac{\Delta\phi}{\Delta\theta}$$
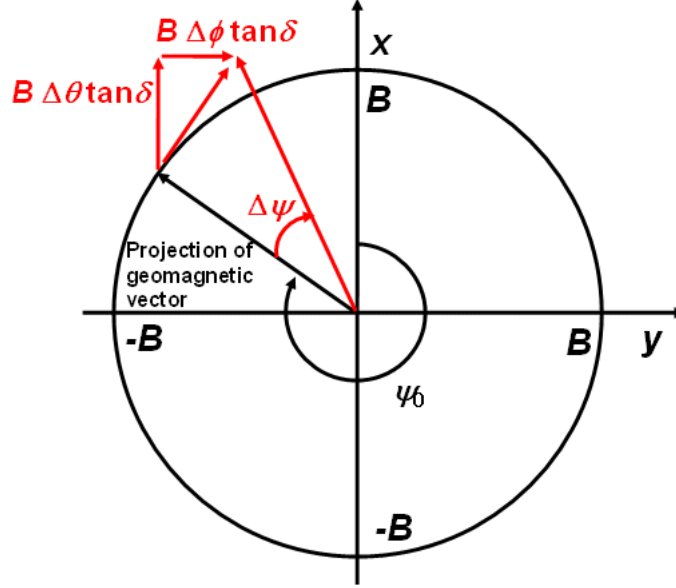
Eqn. 24

Figure 4. Geometry of Accelerometer-Induced Compass Angle Errors

Equation 7 plots Equation 22 for $\Delta\phi tan\,\delta = \Delta\theta tan\,\delta$ with both ranging from 0° to 5° error and for varying ψ_0 between 0° and 360°. As predicted by Equations 23 and 24, the maximum accelerometer induced compass angle error when $\Delta\phi tan\,\delta = \Delta\theta tan\,\delta$ equals 5° is $\Delta\psi_{max} = 5\sqrt{2} = 7.07^o$. Zeroes in $\Delta\psi$ occur as predicted at 45° and 225° where $tan(\Delta\psi) = 1$.

Accelerometer Induced Yaw Angle Errors
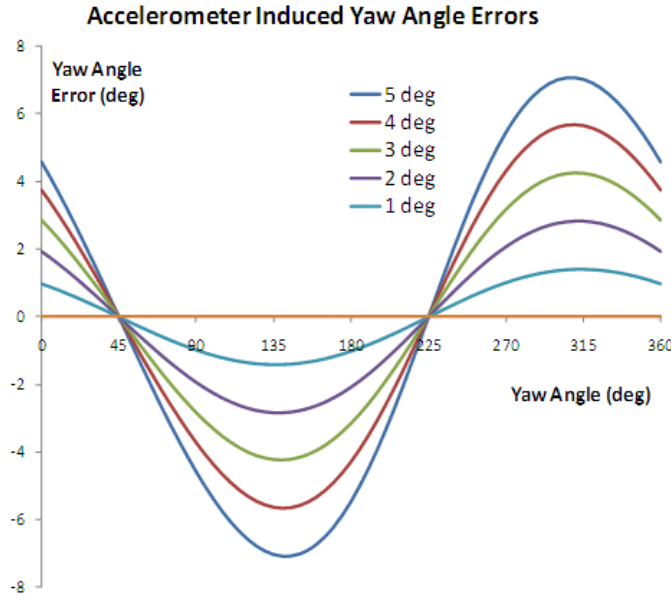
Figure 5. Accelerometer-Induced Compass Angle Errors

6 Hard Iron Magnetic Calibration Induced Errors in Compass Angle

This section derives expressions for the additional errors in the compass heading angle resulting from incomplete removal of hard iron effects by the magnetic calibration algorithms. These magnetometer-induced compass errors add to the accelerometer-induced compass error in Equation 22.

Application note AN4246 contains an explanation of how the zero field offset error in the magnetometer sensor is indistinguishable from a hard iron offset generated by ferromagnetic PCB components and is conventionally calibrated at the same time as the hard iron offset. The term 'hard iron offset' in this section therefore refers to the sum of the ferromagnetic hard iron offset and the magnetometer sensor zero field offset.

For simplicity, and to decouple the discussion from errors in the accelerometer sensor, this section uses a two-dimensional model to examine the effects of incomplete removal of hard and soft iron effects.

AN4248 equation 8 defines the magnetometer sensor output B_p in terms of the true orientation angles and the true hard iron vector V_0 with true components V_{x0}, V_{y0}, V_{z0}. Restricting the magnetometer sensor to be flat with zero roll and zero pitch angle gives:

$$\boldsymbol{B}_p = \begin{pmatrix} B_{px} \\ B_{py} \\ B_{pz} \end{pmatrix} = \boldsymbol{R}_z(\psi_0)B\begin{pmatrix} \cos\delta \\ 0 \\ \sin\delta \end{pmatrix} + \boldsymbol{V}_0 = \begin{pmatrix} B\cos\psi_0\cos\delta + V_{x0} \\ -B\sin\psi_0\cos\delta + V_{y0} \\ \sin\delta + V_{z0} \end{pmatrix} \qquad \textbf{\textit{Eqn. 25}}$$

Accuracy of Angle Estimation in eCompass and 3-D Pointer Applications, Rev. 0

The estimated compass angle ψ is computed from AN4248 equation 22 using the best estimate of the hard iron offset vector V with components V_x, V_y, V_z:

$$tan\,\psi = tan(\psi_0 + \Delta\psi) = \frac{-(B_{py} - V_y)}{(B_{px} - V_x)} = \frac{-\{-B\,sin\,\psi_0\,cos\,\delta - (V_y - V_{y0})\}}{\{B\,cos\,\psi_0\,cos\,\delta - (V_x - V_{x0})\}} \qquad \textbf{Eqn. 26}$$

The terms $(V_x - V_{x0})$ and $(V_y - V_{y0})$ are the errors in the estimation of the components of the hard iron offset. If the calibration algorithms have operated with complete accuracy then $(V_x = V_{x0})$ and $(V_y = V_{y0})$ and Equation 26 simplifies to:

$$\Delta\psi = tan^{-1}\left(\frac{B\,sin\,\psi_0\,cos\,\delta}{B\,cos\,\psi_0\,cos\,\delta}\right) - \psi_0 = 0 \qquad \textbf{Eqn. 27}$$

In the general case, however, there will be a residual error in the estimation by the magnetic calibration algorithms of the hard iron offset. Equation 26 can be written in terms of these residual hard iron errors $\Delta V_x = V_x - V_{x0}$ and $\Delta V_y = V_y - V_{y0}$ as:

$$tan\,\psi = tan(\psi_0 + \Delta\psi) = \frac{sin\,\psi_0 + \left(\frac{\Delta V_y}{B\,cos\,\delta}\right)}{cos\,\psi_0 - \left(\frac{\Delta V_x}{B\,cos\,\delta}\right)} \Rightarrow \Delta\psi = tan^{-1}\left(\frac{sin\,\psi_0 + \left(\frac{\Delta V_y}{B\,cos\,\delta}\right)}{cos\,\psi_0 - \left(\frac{\Delta V_x}{B\,cos\,\delta}\right)}\right) - \psi_0 \qquad \textbf{Eqn. 28}$$

Equation 28 is now in the form of Equation 22 and the results derived from Equation 22 can be re-used. Specifically, errors ΔV_x and ΔV_y will, using a small angle approximation, also produce a sinusoidally varying error $\Delta\psi$ in the estimated compass angle with amplitude $\Delta\psi_{max}$ given in radians by:

$$\Delta\psi_{max} = \sqrt{\left(\frac{\Delta V_x}{B\,cos\,\delta}\right)^2 + \left(\frac{\Delta V_y}{B\,cos\,\delta}\right)^2} = \frac{\sqrt{\Delta V_x^2 + \Delta V_y^2}}{|B\,cos\,\delta|} \qquad \textbf{Eqn. 29}$$

Since compass heading errors resulting from errors in the pitch and roll angles computed from the accelerometer and errors in the estimated hard iron offset both produce a sinusoidal variation in compass error with one cycle per 360°, there is the potential for confusion between these two error sources.

Equation 29 provides the mathematical justification for the statement in Application Note AN4247 that:

"...the lowest value of the horizontal field strength likely to be experienced by a smartphone user is 10 µT in northern Canada and Russia. A compass heading accuracy of 0.05 radians or 3° therefore requires that the error in estimating the geomagnetic field be no more than 0.5 µT".

Substituting the values in the previous paragraph into Equation 29 and, recognizing that $B\,cos\,\delta$ is the horizontal geomagnetic field component, gives the constraint on the maximum permissible error in the estimated hard iron offset for 3° compass accuracy as:

$$\sqrt{\Delta V_x^2 + \Delta V_y^2} < 0.05 \times 10\mu T \Rightarrow \sqrt{\Delta V_x^2 + \Delta V_y^2} < 0.5\mu T \qquad \textbf{Eqn. 30}$$

7 Soft Iron Magnetic Calibration Induced Errors in Compass Angle

Application note AN4926 equation 5 defines the model for the magnetometer output B_p in the presence of the true hard iron vector V_0, true soft iron matrix W_0 and true orientation angles ϕ_0, θ_0, ψ_0 as:

$$B_p = W_0 R_x(\phi_0) R_y(\theta_0) R_z(\psi_0) B \begin{pmatrix} \cos \delta \\ 0 \\ \sin \delta \end{pmatrix} + V_0 \qquad \text{Eqn. 31}$$

If, for simplicity, the model is restricted to soft iron effects only for the two-dimensional configuration $\phi_0 = \theta_0 = 0$ then the magnetometer output is:

$$B_p = W_0 R_z(\psi_0) B \begin{pmatrix} \cos \delta \\ 0 \\ \sin \delta \end{pmatrix} = W_0 \begin{pmatrix} B \cos \psi_0 \cos \delta \\ -B \sin \psi_0 \cos \delta \\ B \sin \delta \end{pmatrix} \qquad \text{Eqn. 32}$$

The locus of the magnetometer readings corrected by the estimated inverse soft iron matrix W^{-1} is:

$$(W^{-1} B_p)^T (W^{-1} B_p) = \left\{ W^{-1} W_0 \begin{pmatrix} B \cos \psi_0 \cos \delta \\ -B \sin \psi_0 \cos \delta \\ B \sin \delta \end{pmatrix} \right\}^T \left\{ W^{-1} W_0 \begin{pmatrix} B \cos \psi_0 \cos \delta \\ -B \sin \psi_0 \cos \delta \\ B \sin \delta \end{pmatrix} \right\} \qquad \text{Eqn. 33}$$

$$\Rightarrow B_p^T (W^{-1})^T W^{-1} B_p = \begin{pmatrix} B \cos \psi_0 \cos \delta \\ -B \sin \psi_0 \cos \delta \\ B \sin \delta \end{pmatrix}^T W_0^T (W^{-1})^T W^{-1} W_0 \begin{pmatrix} B \cos \psi_0 \cos \delta \\ -B \sin \psi_0 \cos \delta \\ B \sin \delta \end{pmatrix} \qquad \text{Eqn. 34}$$

It is trivial to prove that the matrix $W_0^T (W^{-1})^T W^{-1} W_0$ is symmetric. In consequence, Equation 34

defines an ellipsoid (see AN4246 equation 13 for details) and the locus of magnetometer readings corrected by the estimated inverse soft iron matrix W^{-1} lies on the surface of this ellipsoid. If the calibration is perfect, then $W^{-1} W_0 = I$ and the corrected magnetometer values lie on the surface of a sphere. In general, however, the calibration will be slightly imperfect and the corrected values will lie on an ellipsoid which approaches the sphere in the limiting case of perfect calibration.

Figure 6 shows Equation 34 in diagram form. The outer dotted ellipse is the locus of the magnetometer readings B_p distorted by the soft iron matrix W_0 as defined by Equation 32. Perfect calibration using $W^{-1} W_0 = I$ would move the locus to the inner solid circle resulting in no compass heading error. In practice, imperfect calibration correction by W^{-1} where $W^{-1} W_0 \approx I$ moves the locus to the inner ellipsoid defined by Equation 34 with error $\Delta \psi$ in the compass heading angle.
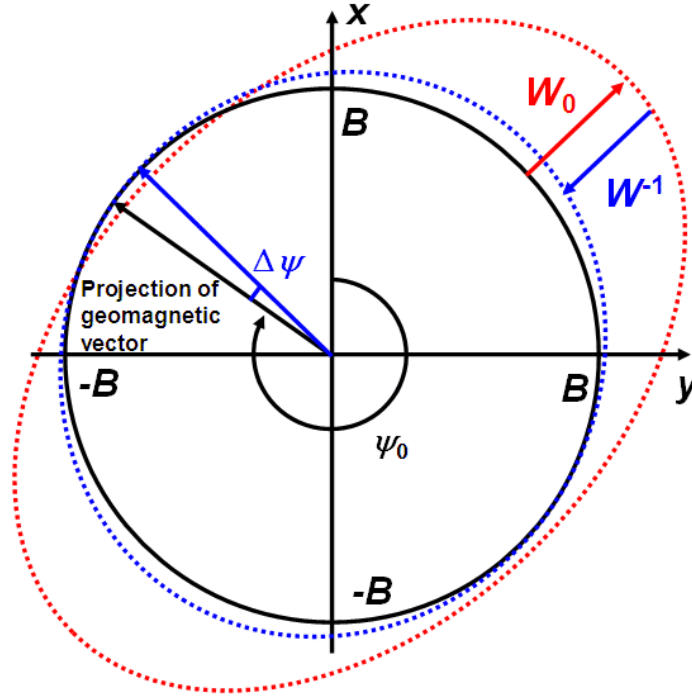
Figure 6. Locus of the Geomagnetic Vector With Imperfect Soft Iron Correction

Visual inspection of Figure 6 shows that the compass error $\Delta\psi$ resulting from imperfect soft iron calibration will vary with two cycles per 360°. The error can easily be computed mathematically by defining $W^{-1}W_0 = I + \Delta W$, where ΔW is a measure of the residual error in the soft iron calibration estimate, and substituting into AN4248 equation 22.

In the two dimensional model we're considering, $I + \Delta W$ can be written as:

$$I + \Delta W = \begin{pmatrix} (1 + \Delta W_{00}) & \Delta W_{01} & 0 \\ \Delta W_{10} & (1 + \Delta W_{11}) & 0 \\ 0 & 1 & 0 \end{pmatrix}$$

Eqn. 35

The error in the estimated compass heading angle is then:

$$\tan\psi = \tan(\psi_0 + \Delta\psi) = \frac{(1 + \Delta W_{11})\sin\psi_0 - \Delta W_{10}\cos\psi_0}{(1 + \Delta W_{00})\cos\psi_0 - \Delta W_{01}\sin\psi_0}$$

Eqn. 36

The right hand side of equation 36 is unchanged when evaluated at compass angles ψ_0 and $\psi_0 + \pi$ which implies that the compass heading error $\Delta\psi$ is equal at angles ψ_0 and $\psi_0 + \pi$. The compass heading error $\Delta\psi$ resulting from incomplete soft iron correction therefore undergoes two cycles per 360°.

Figure 7 shows the explicit calculation of Equation 36 for the case of $\Delta W_{11} = \Delta W_{00} = -\Delta W_{10} = -\Delta W_{01}$ varying from 0 to 0.1 in steps of 0.02.
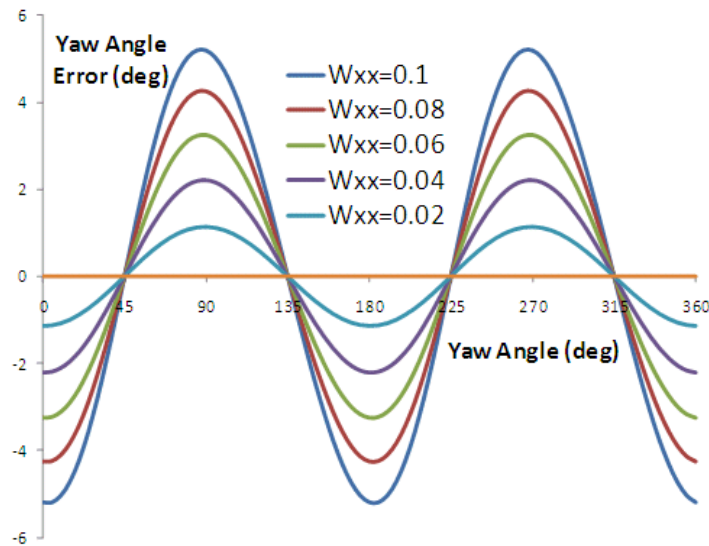
Figure 7. Soft Iron-Induced Compass Angle Errors

The presence of an error signal with two cycles per 360° is characteristic of soft iron calibration errors.

8 Extension to Time Varying Sensor Errors

The previous sections of this document have calculated roll, pitch and compass angle errors as a function of known errors in the accelerometer and magnetometer sensor outputs. Since the sensor outputs will have both a DC and a random time varying component, the previous results apply either to i) time averaged angle errors as a function of the DC component of the sensor outputs or ii) to instantaneous angle errors at a specific time.

This section therefore extends the discussion to time varying sensor error outputs and shows how these are defined by parameters listed in the data sheets. Finally, the effect of any digital filtering is discussed since this will, in general, change the statistics of the sensor outputs and the statistics of the angle errors.

8.1 Accelerometer Zero-g Offset

An accelerometer data sheet will specify a 'zero-g offset level' error which is the accelerometer channel reading under conditions of zero acceleration or zero gravity where the correct reading should be zero. The zero-g offset level is therefore a fixed DC offset for a given accelerometer channel. Different accelerometer channels will have different DC offsets.

The data sheet for the Freescale MMA8451 three axis accelerometer specifies a zero-g offset for each axis as being independently distributed in the range ±20 mg before board mount and increasing to ±30 mg after board mount as a result of the thermal stresses in the soldering process.

The zero-g offset will also vary with temperature. For the MMA8451, Freescale specifies a typical distribution range of ±0.15 mg/C for the zero-g offset over the operating range -40°C to 85°C.

To a good approximation, accelerometer sensors have a linear response to acceleration or gravity so that the zero-g offset for a specific channel of a specific sensor at a particular temperature will also be an additive offset over the entire operating range of that sensor channel. For example, if the *y*-channel zero-g offset of a specific MMA8451 accelerometer is -18.45 mg at 30C after mounting on a PCB then an additive correction of +18.45 mg should be applied to any *y* axis acceleration measurement at 30°C temperature for that part.

8.2   Magnetometer Zero-Field Offset

The corresponding figure for a magnetometer sensor is the 'zero field' offset which is the output in the absence of any magnetic field. For reasons explained in Application Note AN4246, the zero field offset error simply adds to the PCB hard iron offset and is normally calibrated away at the same time. It is therefore common practice among magnetometer sensor suppliers to not calibrate the zero-field offset during manufacture.

8.3   Accelerometer Noise Figure

Accelerometer noise is typically specified as a noise amplitude *A* measured in µg per $\sqrt{\text{Hz}}$ for a specific output data rate. The Freescale MMA8451, for example, has a noise amplitude *A* of 126 µg per $\sqrt{\text{Hz}}$ at an output data rate of 400 Hz.

The noise amplitude is difficult to understand physically because of its units of µg per $\sqrt{\text{Hz}}$. Squaring the noise amplitude *A*, however, gives the noise power density *P* measured in g^2 per Hz which is physically understandable as the distribution of noise power with frequency. The MMA8451 noise amplitude of $A = 126$ µg per $\sqrt{\text{Hz}}$ translates to a uniform noise power density of $P = 1.59 \times 10^{-8} g^2$ per Hz. The flat spectrum implies that the accelerometer noise spectrum is white with noise values uncorrelated from one output sample to the next.

The corresponding noise amplitude σ in the time domain can be determined by simply equating the integral of noise power density *P* between DC and the Nyquist frequency (equal to half the accelerometer output sampling frequency f_s) to the noise power σ^2 in the time domain:

$$\sigma^2 = \int_0^{f_{Nyq}} P df = \int_0^{\frac{f_x}{2}} P df = P f_{Nyq} \Rightarrow \sigma = \sqrt{P f_{Nyq}} = A \sqrt{f_{Nyq}} \qquad \textit{Eqn. 37}$$

Equation 37 justifies the mathematical shortcut of multiplying the noise amplitude density *A* by the square root of the Nyquist frequency to obtain the RMS noise amplitude σ in the time domain.

Applying Equation 37 to the Freescale MMA8451 at 400 Hz sampling rate (and 200 Hz Nyquist frequency) gives an integrated noise power of $200 \times 1.59 \times 10^{-8} g^2 = 3.18 \times 10^{-6} g^2$ and an RMS noise amplitude σ equal to 1.78 mg. The same result for σ can be obtained using the shortcut to multiply the noise amplitude *A* by the square root of the Nyquist frequency to give 126 µg x 14.14 which also equals 1.78 mg.

8.4   Magnetometer Noise Figure

The magnetometer noise is commonly specified directly as an RMS amplitude for specified output sampling rates. For the Freescale MAG3110 magnetometer, for example, the output noise in each channel is 0.25 µT RMS at 10 Hz output data rate rising to 0.4 µT at 80 Hz output rate.

8.5   Sensor Noise Statistics

The model for the error component of a specific accelerometer or magnetometer channel $x[n]$ is therefore the sum of DC term µ and a zero mean, unit variance, white noise process $u[n]$ scaled to have variance σ^2:

$$x[n] = \mu + \sigma u[n]$$ **Eqn. 38**

$x[n]$ is therefore equivalent to the instantaneous accelerometer or magnetometer error referred to in earlier sections.

It is additionally assumed that the sensor noise has a Normal distribution $N(\mu, \sigma^2)$. Integrating this distribution gives the probability of measurements lying within one, two and three standard deviations of the mean:

$$p(-\sigma, \sigma) = \frac{1}{\sigma\sqrt{2\pi}}\int_{-\sigma}^{\sigma} e^{\frac{-(x-\mu)^2}{2\sigma^2}} dx = erf\left(\frac{1}{\sqrt{2}}\right) = 68.3\%$$ **Eqn. 39**

$$p(-2\sigma, 2\sigma) = \frac{1}{\sigma\sqrt{2\pi}}\int_{-2\sigma}^{2\sigma} e^{\frac{-(x-\mu)^2}{2\sigma^2}} dx = erf\left(\frac{2}{\sqrt{2}}\right) = 95.5\%$$ **Eqn. 40**

$$p(-3\sigma, 3\sigma) = \frac{1}{\sigma\sqrt{2\pi}}\int_{-3\sigma}^{3\sigma} e^{\frac{-(x-\mu)^2}{2\sigma^2}} dx = erf\left(\frac{3}{\sqrt{2}}\right) = 99.7\%$$ **Eqn. 41**

68.3% of measurements derived from a Normal distribution lie between ± one standard deviation, 95.5% within ± two standard deviations and 99.7% within ± three standard deviations of the mean. For the example of the MMA8451 at a sampling rate of 400 Hz, 95.5% of measurements will lie within a range of ±2 x 1.78 mg = ±3.56 mg of the mean.

Occasionally an accelerometer noise figure will be specified in terms of bit counts. The Freescale MMA7660 is a 6-bit accelerometer with range ±1.5g. The sensitivity is therefore 32 / 1.5g = 21.33 bits/g. The noise level for the MMA7660 is defined as ±1 bit or ±46.88 mg for 94% of measurements. On the assumption of a Normal distribution, the RMS noise amplitude for the MMA7660 will be approximately 23 mg.

It cannot be assumed that the resulting error angles are Normally distributed just because the accelerometer or magnetometer noise is Normally distributed. But, since the mapping from sensor error to angle error is monotonic, it can be assumed that 68.3%, 95.5% and 99.7% of angle errors will be within the limits computed by inserting one, two and three standard deviation sensor errors into the appropriate equations.

8.6   Effects of Digital Filtering

Sensor noise levels are commonly reduced by low pass filtering. The general input-output difference equation for an arbitrary causal digital filter with transfer function $H(z)$ is:

$$y[n] = \sum_{i=0}^{N-1} h[i]x[n-i]$$

Eqn. 42

Equation 42 applies both to finite impulse response filters (N finite) and infinite impulse response filters (N unbounded). The transfer function $H(z)$ is defined as:

$$H[z] = \sum_{i=0}^{N-1} h[i]z^{-i}$$

Eqn. 43

If $x[n]$ is the noise process defined in Equation 38 then the power of the output series $y[n]$ is (where E{} is the expectation operator):

$$E\{y[n]^2\} = E\left\{\sum_{i=0}^{N-1} h[i]x[n-i]\sum_{j=0}^{N-1} h[j]x[n-j]\right\} = \sum_{i=0}^{N-1}\sum_{j=0}^{N-1} h[i]h[j]E\{x[n-i]x[n-j]\}$$

Eqn. 44

$$\Rightarrow E\{y[n]^2\} = \sum_{i=0}^{N-1}\sum_{j=0}^{N-1} h[i]h[j]E\{\mu^2 + \sigma^2 u[n-i]u[n-j]\} = \mu^2\left\{\sum_{i=0}^{N-1} h[i]\right\}^2 + \sigma^2\sum_{i=0}^{N-1} h[i]^2$$

Eqn. 45

The noise power is therefore reduced by the filter power gain factor $\sum_{i=0}^{N-1} h[i]^2$. As a specific example, a simple 5 element finite impulse response low pass filter with elements (1/5, 1/5, 1/5, 1/5, 1/5) reduces the power of a zero mean white noise process by a factor of 5 and reduces the amplitude by a factor of $\sqrt{5}$. The effects of any such filtering on the statistics of the sensor output must be included before calculating the statistics of the resulting angle errors.

How to Reach Us:

Home Page:
www.freescale.com

Web Support:
http://www.freescale.com/support

USA/Europe or Locations Not Listed:
Freescale Semiconductor, Inc.
Technical Information Center, EL516
2100 East Elliot Road
Tempe, Arizona 85284
1-800-521-6274 or +1-480-768-2130
www.freescale.com/support

Europe, Middle East, and Africa:
Freescale Halbleiter Deutschland GmbH
Technical Information Center
Schatzbogen 7
81829 Muenchen, Germany
+44 1296 380 456 (English)
+46 8 52200080 (English)
+49 89 92103 559 (German)
+33 1 69 35 48 48 (French)
www.freescale.com/support

Japan:
Freescale Semiconductor Japan Ltd.
Headquarters
ARCO Tower 15F
1-8-1, Shimo-Meguro, Meguro-ku,
Tokyo 153-0064
Japan
0120 191014 or +81 3 5437 9125
support.japan@freescale.com

Asia/Pacific:
Freescale Semiconductor China Ltd.
Exchange Building 23F
No. 118 Jianguo Road
Chaoyang District
Beijing 100022
China
+86 10 5879 8000
support.asia@freescale.com

For Literature Requests Only:
Freescale Semiconductor Literature Distribution Center
1-800-441-2447 or +1-303-675-2140
Fax: +1-303-675-2150
LDCForFreescaleSemiconductor@hibbertgroup.com